ISSN 1674-1056
http://cpb.iphy.ac.cn
http://iopscience.iop.org/cpb
中国物理 B
Chinese Physics
中国物理 Chinese Physics B

Topological Anderson insulator in two-dimensional non-Hermitian systems

Hongfang Liu(刘宏芳), Zixian Su(苏子贤), Zhi-Qiang Zhang(张智强), Hua Jiang(江华)
Citation: Chin. Phys. B . 2020, 29(5): 050502 . **doi:** 10.1088/1674-1056/ab8201
Journal homepage: http://cpb.iphy.ac.cn; http://iopscience.iop.org/cpb

What follows is a list of articles you may be interested in

Evacuation simulation considering action of guard in artificial attack

Chang-Kun Chen(陈长坤), Yun-He Tong(童蕴贺)
Chin. Phys. B . 2019, 28(1): 010503 . **doi:** 10.1088/1674-1056/28/1/010503

Recursion-transform method and potential formulae of the *m*×*n* cobweb and fan networks

Zhi-Zhong Tan(谭志中)
Chin. Phys. B . 2017, 26(9): 090503 . **doi:** 10.1088/1674-1056/26/9/090503

Magnetic phase diagrams of Fe-Mn-Al alloy on the Bethe lattice

Erhan Albayrak
Chin. Phys. B . 2017, 26(2): 020502 . **doi:** 10.1088/1674-1056/26/2/020502

Two-point resistance of an *m*×*n* resistor network with an arbitrary boundary and its application in RLC network

Zhi-Zhong Tan(谭志中)
Chin. Phys. B . 2016, 25(5): 050504 . **doi:** 10.1088/1674-1056/25/5/050504

Recursion-transform approach to compute the resistance of a resistor network with an arbitrary boundary

Tan Zhi-Zhong
Chin. Phys. B . 2015, 24(2): 020503 . **doi:** 10.1088/1674-1056/24/2/020503

SPECIAL TOPIC — Topological 2D materials

Topological Anderson insulator in two-dimensional non-Hermitian systems*

Hongfang Liu(刘宏芳)[1], Zixian Su(苏子贤)[1], Zhi-Qiang Zhang(张智强)[1,†], and Hua Jiang(江华)[1,2,‡]

[1] School of Physics and Technology, Soochow University, Suzhou 215006, China
[2] Institute for Advanced Study, Soochow University, Suzhou 215006, China

(Received 2 January 2020; revised manuscript received 15 February 2020; accepted manuscript online 23 March 2020)

We study the disorder-induced phase transition in two-dimensional non-Hermitian systems. First, the applicability of the noncommutative geometric method (NGM) in non-Hermitian systems is examined. By calculating the Chern number of two different systems (a square sample and a cylindrical one), the numerical results calculated by NGM are compared with the analytical one, and the phase boundary obtained by NGM is found to be in good agreement with the theoretical prediction. Then, we use NGM to investigate the evolution of the Chern number in non-Hermitian samples with the disorder effect. For the square sample, the stability of the non-Hermitian Chern insulator under disorder is confirmed. Significantly, we obtain a nontrivial topological phase induced by disorder. This phase is understood as the topological Anderson insulator in non-Hermitian systems. Finally, the disordered phase transition in the cylindrical sample is also investigated. The clean non-Hermitian cylindrical sample has three phases, and such samples show more phase transitions by varying the disorder strength: (1) the normal insulator phase to the gapless phase, (2) the normal insulator phase to the topological Anderson insulator phase, and (3) the gapless phase to the topological Anderson insulator phase.

Keywords: disorder effect, topological Anderson insulator, non-Hermitian systems

PACS: 05.50.+q, 03.65.Vf **DOI:** 10.1088/1674-1056/ab8201

1. Introduction

Since the spin Hall model proposed by Kane and Mele in 2005,[1–3] topological states based on Hermitian systems have been greatly developed.[4–13] Among them, ten classes of topological phases guaranteed by time-reversal symmetry, inversion symmetry, and particle–hole symmetry are the vital research objects.[3,14–16] With the help of the space group and the point group, topological crystalline insulators were also proposed by Fu.[17] These topological states receive great interest over the past few years.[18–25] Very recently, three groups[26–28] extended the study of topological states in Hermitian systems to the complete inorganic crystal structure database.

With the comprehensive understanding of the topological states in Hermitian systems, physicists begin to suspect whether topological states exist in non-Hermitian systems as well.[29] For Hermitian systems, the topological order is mainly determined by the bulk states.[3,5,30] To be specific, the bulk–edge correspondence[3,5] is achieved. This method was also widely used in early studies of non-Hermitian systems.[31–40] Nevertheless, several studies illustrated that non-Hermitian systems could be completely different from the Hermitian ones[33–36] in their unique property — the non-Hermitian skin effect,[41–43] which means that all the eigenstates concentrate on one side or even one point of the samples' open boundary. This characteristic makes the topological properties of the open boundary conditions in the non-Hermitian system notably different from the periodic boundary case.[34–36] For example, the emergence of zero energy state is regarded as the benchmark to define the topological state in the one-dimensional model for both Hermitian[44–47] and non-Hermitian[32] systems. It is believed that the winding number,[46,47] which is calculated by the bulk states of a sample with the periodic boundary condition, will determine the existence of zero-energy modes and give a reasonable phase diagram. However, the distribution of zero energy states obtained with the open boundary samples is quite different from that with the periodic boundary condition in non-Hermitian systems.[33–35] To determine the topological phase diagram of non-Hermitian systems, Yao *et al.* proposed a special transformation to the non-Hermitian Hamiltonian.[35,36] After such a kind of transformation, the effective Hamiltonian becomes Hermitian at high symmetric points. When a phase transition happens, the bandgap at a high symmetric point is closed and then reopened. Therefore, the correct phase boundaries can be obtained. These works significantly advanced the study of topological states in non-Hermitian systems.

Notably, the effect of disorder is inevitable in experi-

*Project supported by the National Basic Research Program of China (Grant No. 2019YFA0308403), the National Natural Science Foundation of China (Grant No. 11822407), Undergraduate Training Program for Innovation and Entrepreneurship, Soochow University (Grant No. 201810285022Z), and a Project Funded by the Priority Academic Program Development of Jiangsu Higher Education Institutions, China.

†Corresponding author. E-mail: zqzhang2018@stu.suda.edu.cn
‡Corresponding author. E-mail: jianghuaphy@suda.edu.cn

© 2020 Chinese Physical Society and IOP Publishing Ltd

ments because there always exist impurities or non-uniformity in the samples. After the pioneering work by Anderson *et al.*,[48] the study of disorder effect has received extensive advancement.[49–51] For a long period, disorder is considered to make things worse, e.g., the Anderson localization.[49–56] However, an unexpected phase transition induced by disorder was reported in 2009,[57,58] in which disorder can turn a normal insulator into a topological insulator. Such a nontrivial phase induced by disorder is called the topological Anderson insulator, and has been widely studied in the Hermitian system.[57–60] Since all systems could have impurities, it is also essential to study the disorder effect for non-Hermitian systems. Previously, the disorder in non-Hermitian systems was investigated in terms of the distribution of eigenvalues.[61–63] These works mainly focus on the stability of the topological states, but the investigation of the interplay between TAI and the non-Hermitian effect is still insufficient.

In this paper, the disorder-induced topological phase transition of the non-Hermitian insulator is numerically studied with the help of noncommutative geometric method (NGM).[46,47,54,55,64,65] We first investigate the applicability of NGM in non-Hermitian systems for two different cases (the effective model in periodic boundary condition and the original model in open boundary condition). These two cases show the coincident phase transition points, which agrees quite well with the analytical one. We also find that the Chern number calculated by NGM slightly deviates from the quantized value (the maximum deviation is about 0.1) when the non-Hermitian effect appears, and the deviation could be eliminated by enlarging the sample size. Next, after checking the stability of the numerical method, the disorder effect in non-Hermitian systems is considered. We confirm that non-Hermitian Chern insulators are robust against disorder. Meanwhile, the disorder makes non-Hermitian systems transform from the trivial phase to the nontrivial phase, which is similar to the topological Anderson transition in Hermitian systems. Finally, cylindrical samples are investigated, and they show more phase transitions.

2. Model and method

The first selected non-Hermitian Hamiltonian is[36]

$$H = (vk_x + \mathrm{i}\gamma)\sigma_x + (vk_y + \mathrm{i}\gamma)\sigma_y + \left(m - 2t + \frac{tk_x^2}{2} + \frac{tk_y^2}{2}\right)\sigma_z. \tag{1}$$

According to the non-Bloch theory for a square sample, the replacement $\boldsymbol{k} \to \tilde{\boldsymbol{k}} - \mathrm{i}\gamma/v$ leads to[36]

$$\begin{aligned} H_{\text{eff}} &= v\tilde{k}_x\sigma_x + v\tilde{k}_y\sigma_y \\ &+ \left(m - 2t - \gamma^2 + \frac{t\tilde{k}_x^2 + t\tilde{k}_y^2}{2} - \mathrm{i}\frac{t\gamma\tilde{k}_x + t\gamma\tilde{k}_y}{v}\right)\sigma_z. \end{aligned} \tag{2}$$

It is obvious that H_{eff} is Hermitian Hamiltonian when $\tilde{k}_x = 0$ and $\tilde{k}_y = 0$, which is helpful to give the correct phase boundary. In the process of replacement, the bulk states of H_{eff} can also effectively exhibit the bulk properties of H under the open boundary condition.[36]

As shown in Figs. 1(a)–1(c), $\mathrm{Re}(E)$ (the real part of the eigenvalues) versus $\mathrm{Im}(E)$ (the imaginary part of the eigenvalues) under three different conditions are plotted for a square sample with size $N = 50$, $\gamma = 0.4$, and $m = 1.7$. In the following numerical calculation, we set $v = 1$ and $t = 1$ for simplicity. Figure 1(a) is obtained with H_{eff} under the periodic boundary condition. The bandgap of $\mathrm{Re}(E)$ shown in Fig. 1(a) (marked in cyan) is the same as the result of H under the open boundary condition (see Fig. 1(b)). It is obvious that the plots of $\mathrm{Re}(E)$ versus $\mathrm{Im}(E)$ under periodical boundary case of H_{eff} and open boundary case of H are different from the case of H under the periodic boundary condition (see Fig. 1(c)). For instance, the latter case has no gap for $\mathrm{Re}(E)$. These results are consistent with the previous study.[36] Furthermore, the periodical boundary of H_{eff} has exhibited the main properties of the real part of the open boundary of H. Although $\mathrm{Re}(E)$ versus $\mathrm{Im}(E)$ for H_{eff} under the condition of the periodic boundary slightly deviates from the distribution of H under the condition of the open boundary, the phase transition in these two cases could be the same. The reason can be simplified that the topological phase transition is characterized by the bandgap evolution of the real part of the eigenvalues.[66] Furthermore, we also calculate the eigenvalue of H under the periodical boundary condition with $m = 2.7$ (trivial insulator phase). As shown in Fig. 1(d), there are no edge states in the bulk gap.

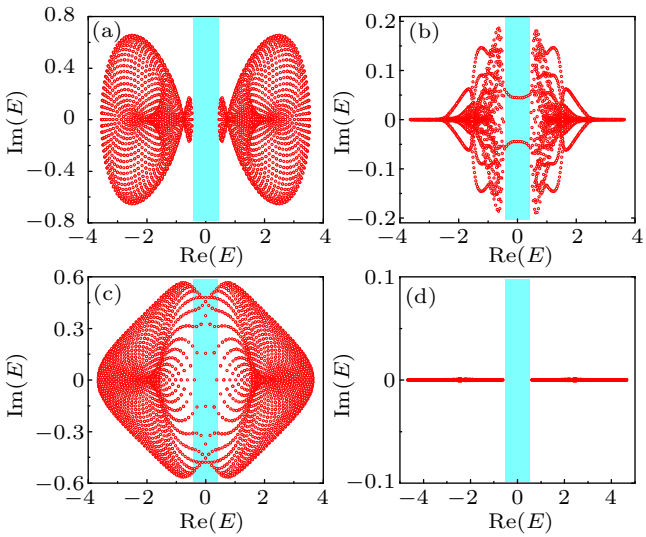


Fig. 1. The $\mathrm{Re}(E)$ versus $\mathrm{Im}(E)$ with (a)–(c) $m = 1.7$ and (d) $m = 2.7$, respectively. E is the eigenvalue of a square sample. Other parameters are fixed at $\gamma = 0.4$ and $N = 50$. (a) The periodic boundary of H_{eff}. (b), (d) The open boundary of H with $m = 1.7$ (b) and $m = 2.7$ (d). (c) The periodic boundary of H.

To better understand the difference between H under the condition of the open boundary and H_{eff} under the condition of the periodic boundary, we compare the Chern numbers for these two cases. The Chern number for the finite-sized sample

is calculated by combining the generalized definition of non-Bloch Chern number[36] and the theory of Chern number in real space.[64,65] Due to the non-Hermitian properties of the Hamiltonian, the eigenvalues of H and $H^\dagger$ are separately defined as[36]

$$H|u_{\mathrm{R}\alpha}\rangle = E_\alpha|u_{\mathrm{R}\alpha}\rangle,\ \ H^\dagger|u_{\mathrm{L}\alpha}\rangle = E_\alpha^*|u_{\mathrm{L}\alpha}\rangle, \tag{3}$$

where $|u_{\mathrm{R}\alpha}\rangle$ and $|u_{\mathrm{L}\alpha}\rangle$ are the standard right and left eigenvectors, respectively. Except for the singularity, the above formulas are well defined. Different from the Hermitian systems, the completeness of the system requires that the standard right and left eigenvectors meet the normalization relation $\langle u_{\mathrm{L}\alpha}|u_{\mathrm{R}\beta}\rangle = \delta_{\alpha\beta}$. The transformation matrix V formed by the standard right eigenvectors is a specific transformation with $V^{-1}HV = J$, where J is the diagonal matrix formed by the eigenvalue E_α. As the eigenvector of H, every column vector of V is the standard right eigenvector of H. The conjugation of $V^{-1}HV = J$ shows $V^\dagger H^\dagger (V^\dagger)^{-1} = J^*$, and every column vector of $(V^\dagger)^{-1}$ is the corresponding standard left eigenvector. It is easy to prove the orthogonality normalization relations between the standard right eigenvectors and the left eigenvectors.

The above eigenvectors can be used to define the non-Bloch Chern number[36,67]

$$\tilde{C} = \frac{1}{2\pi \mathrm{i}} \int_{\mathrm{BZ}} \mathrm{d}^2\tilde{k}\, \mathrm{Tr}\left[P_\alpha \left[\partial_{\tilde{k}_x} P_\alpha, \partial_{\tilde{k}_y} P_\alpha\right]\right], \tag{4}$$

which follows the method in Hermitian. However, the projection operator is redefined as $P_\alpha = |u_{\mathrm{R}\alpha}\rangle\langle u_{\mathrm{L}\alpha}|$. Actually, if one can numerically obtain $\partial_{\tilde{k}_{x(y)}} P_\alpha$, the Chern number is available. For NGM, the crucial equation is $P_k = \sum_{n\in\mathrm{BZ}} b_n \mathrm{e}^{\mathrm{i}kn}$.[64,65] Since the introduced attenuation factor γ/v is a constant, one only needs to transform k into $\tilde{k}$ for non-Hermitian systems. The projection operator in non-Hermitian cases can be expressed as follows:

$$P_{\tilde{k}} = \sum_{n\in\mathrm{BZ}} b_n \mathrm{e}^{\mathrm{i}\tilde{k}n}, \tag{5}$$

where $\partial_{\tilde{k}} P_\alpha$ can be approximately solved, and the detailed analysis of NGM can be obtained in the papers.[46,47,54,64,65] On the other hand, if one assumes that the momentum of H under the condition of the open boundary has no decay terms (γ is a constant in H and independent of k_x and k_y), these terms naturally originate from the non-Hermitian skin effect of the system under the open boundary condition. Then, the Chern number defined by k_x and k_y reads

$$C = \frac{1}{2\pi \mathrm{i}} \int_{\mathrm{BZ}} \mathrm{d}^2 k\, \mathrm{Tr}\left[P_\alpha \left[\partial_{k_x} P_\alpha, \partial_{k_y} P_\alpha\right]\right]. \tag{6}$$

Here, based on the evolution of the Chern number (calculated by Eq. (4) of H_{eff} under the condition of periodic boundary and by Eq. (6) of H under the condition of open boundary), we manifest evidence that the above two cases can give the same transition point. As shown in Fig. 2(a), we plot the Chern number versus m for H under the condition of open boundary and H_{eff} under the condition of periodic boundary with $\gamma = 0.4$. Due to the influence of the eigenvalues inside the bulk gap (see Fig. 1(b)), the Chern number of H under the condition of open boundary is unable to reach the quantized value for nontrivial systems (some topological features determined by the bulk states are lost because the existence of edge states). For trivial systems, the Chern number can capture the zero value because such states are absent (see Fig. 1(d)). For H_{eff} under the condition of periodic boundary, the influence of the edge states to the definition of Chern number can be avoided, the quantized Chern number is achieved (see Fig. 1(a)).

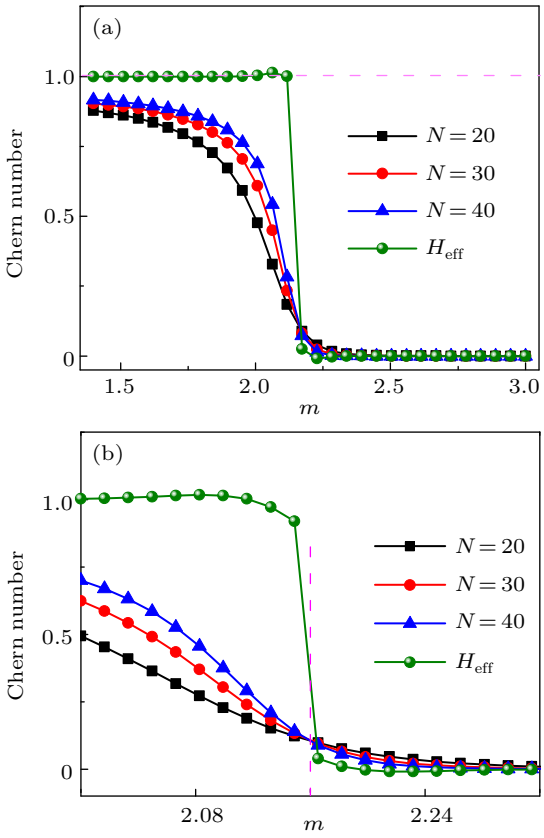


Fig. 2. (a), (b) Chern number evolutions with m for H under the condition of open boundary ($N = 20, 30, 40$) and for H_{eff} under the condition of periodic boundary with $N = 40$, respectively. Panel (b) is zoom of (a) near the transition point. Other parameters are $\gamma = 0.4$, $v = 1$, and $t = 1$. In all the Chern number calculations, we fix the Fermi energy at $E_{\mathrm{F}} = 0$.

In order to make the phase transition point more accurate, we compact the grid near the phase transition point (see Fig. 2(b)). For H under the condition of the open boundary, the scaling behavior of the Chern number under different sample sizes is obtained. With the increasing size, the bulk states become dominant, and the Chern number tends to be quantized. It is found that the phase transition point is near $m = 2.16$ for H under the condition of the open boundary. For H_{eff} under the condition of the periodic boundary, the transition point can be obtained when the Chern number is approximately equal to 0.5, and this position is also around $m = 2.16$. These two conditions are in good agreement with the analytical result

$m = 2+\gamma^2$ with $\gamma = 0.4$. Although the Chern number given by H under the condition of the open boundary can characterize the topological properties of the system more reasonable, it is hard for the Chern number to reach the quantized value because of the redundant states inside the bulk gap (see Fig. 1(b)). Moreover, H_{eff} under the condition of the periodic boundary combined with non-Bloch Chern number can also predict a phase transition point quite well. Therefore, we mainly consider H_{eff} under the condition of the periodic boundary in the following calculations.

3. The stability of the noncommutative geometric method

In the above section, we have shown that the phase transition point obtained by combining H_{eff} under the condition of periodic boundary with NGM is consistent with the analytical prediction. However, more data is needed to ensure whether the feature will hold for the whole parameter regions or not. Sequentially, we study the reliability of NGM for non-Hermitian systems with different γ.

In Fig. 3(a), we obtain a phase diagram based on the Chern number, where the Chern number in the yellow region approximately equals to one (nontrivial), and the Chern number in the blue area is zero (trivial). Furthermore, the red solid line corresponds to the theoretically predicted phase boundary with $m = 2+\gamma^2$.[36] The Chern number distribution agrees perfectly with the theoretical prediction in a wide range of parameters. However, we also find some unexpected values of the Chern number near the phase transition points. The Chern number for systems with strong non-Hermitian features deviates from the quantized value, specifically, it becomes greater than one (Fig. 3(a) in the grey area) or less than zero (Fig. 3(a) in the black area). For smaller γ, these behaviors still hold (see Fig. 2(a)). Since the diagonalization of the non-Hermitian Hamiltonian could be inaccurate,[33] we also calculate $V^{-1}HV - J$ for each sample to eliminate the possibility. Figures 3(c) and 3(d) are the trace of the absolute value of $V^{-1}HV - J$ and the sum of all the non-diagonal terms, respectively. According to the results shown in Figs. 3(c) and 3(d), the deviation of the diagonal elements of $V^{-1}HV$ from J is less than 10^{-8}, and the deviation of the non-diagonal elements from zero is less than 10^{-12}. It implies that the diagonalization of the non-Hermitian matrices is accurate and correct.

To explain this phenomenon, we plot the evolution of the Chern number with the change of sample size N for $\gamma = 0.6$ (Fig. 3(b)). Obviously, except for the phase transition points, the Chern number tends to approach the quantized values by increasing N. Based on the equation $P_k = \sum_{n\in \text{BZ}} b_n e^{ikn}$ in NGM, one can approximately obtain the value of $\partial_{k_x(y)} P_k$ with high accuracy.[64,65] We suspect the singular value of the Chern number is due to the fact that $P_{\tilde{k}} = \sum_{n\in \text{BZ}} b_n e^{i\tilde{k}n}$ could be inaccurate in non-Hermitian systems. Thus, it leads to the reduction of the accuracy of the Chern number. As the size of the sample increases, $P_{\tilde{k}} = \sum_{n\in \text{BZ}} b_n e^{i\tilde{k}n}$ could be much reliable and makes the results more accurate.

Conclusively, the numerical results obtained by combining NGM and non-Bloch Chern number can characterize the topological phase transition. However, when the non-Hermitian features are strong, especially when the parameters are close to the phase transition point, a sample with a large size is needed to achieve reliable results.

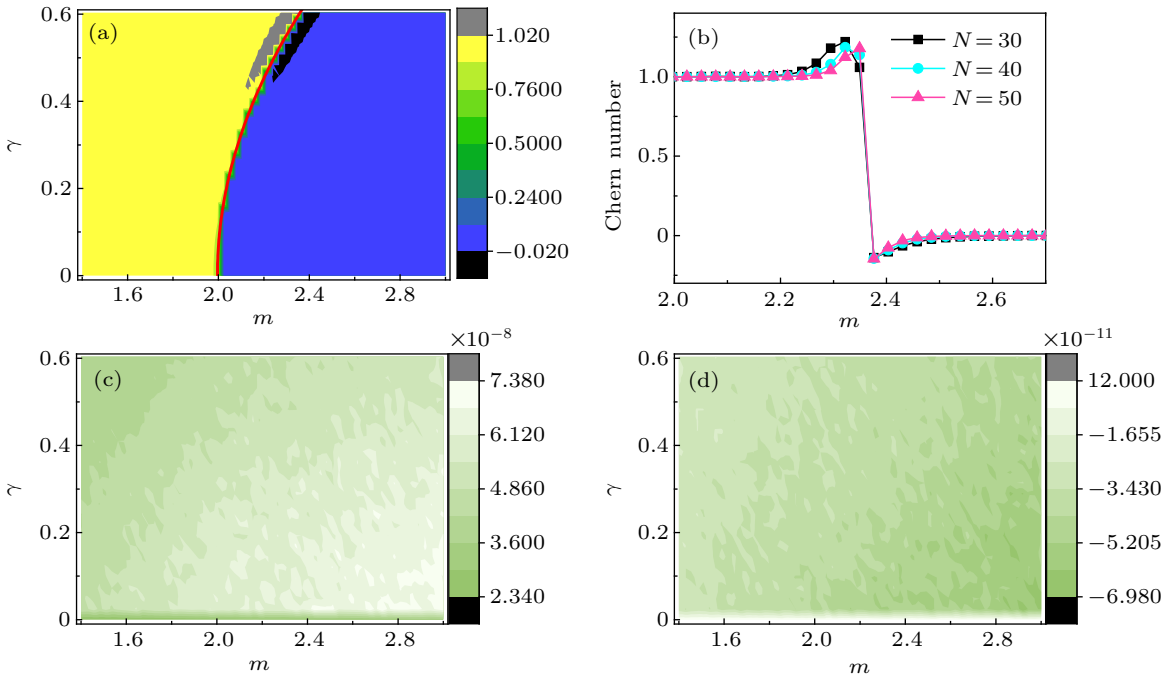


Fig. 3. (a) Chern number versus m and γ with sample size $N = 30$. The red solid line corresponds to the analytical prediction. (b) The selected plot of (a) by setting $\gamma = 0.6$ for different sample size N. (c) and (d) The absolute value of $V^{-1}HV - J$ in the diagonal direction and the sum of the remaining matrix elements, respectively. The value larger (smaller) than the maximum (minimum) value of the color bar is marked by grey (black) color. The other parameters are the same as those in Fig. 2.

4. Topological Anderson insulator in square samples

The established NGM does not require the translation symmetry of the system; thus it has an advantage when dealing with the disorder systems. In this section, we use NGM to investigate the disorder-induced phase transition in two-dimensional non-Hermitian systems. Notably, we examine whether topological Anderson insulators can exist in non-Hermitian systems. In our calculations, the disorder effect is based on the standard Anderson disorder.[48–51] The random on-site energy for each site satisfies the unitary distribution $[-W/2, W/2]$, where W represents the disorder strength.

Since NGM is not suitable to calculate the Chern number in systems with strong non-Hermitian features, we only study the case with small γ ($\gamma = 0.4$). The main results are shown in Fig. 4. In the absence of disorder ($W = 0$), the system is topological nontrivial with Chern number equal to one for $m < 2.16$, and is trivial with zero Chern number when $m > 2.16$. Figure 4(a) plots the Chern number versus both m and disorder strength W for H_{eff} under the condition of the periodic boundary. When $m < 2.16$, the Chern number does not change until $W > 4$. A typical case is given in Fig. 4(b) with $m = 1.5$. It is obvious that the Chern number gradually deviates from the quantized value and tends to zero when disorder strength W exceeds 4.1. These observations demonstrate the stability of the non-Hermitian Chern insulators under disorder.

Interestingly, when $m > 2.16$, the clean samples are normal insulators initially. However, the nontrivial region occurs in a wide range of disorder strength (see Fig. 4(a)). A typical curve is also plotted in Fig. 4(b) with $m = 2.2$. The Chern number remains zero when $W < 1.8$, which indicates the trivial nature of the clean sample. It starts to increase and reaches the quantized value as the disorder strength increases. The quantized plateau maintains in the range of $2.5 < W < 4.2$, where the sample should be attributed to the topological Anderson insulator.

The Chern number gradually decreases to zero when $W > 4.2$, which means the system transmits from the topological Anderson insulator to normal Anderson insulator due to Anderson localization. In order to further study the numerical results obtained by H_{eff} under the periodical boundary conditions, we also investigate the disorder effect of H under the open boundary conditions. As shown in Figs. 4(c) and 4(d), for the same parameters, the trend of the Chern number is consistent with the result of H_{eff} under the condition of the periodic boundary except that the Chern number cannot reach the absolute quantized value. In other words, we reconfirm the topological Anderson phase induced by disorder in the non-Hermitian systems.

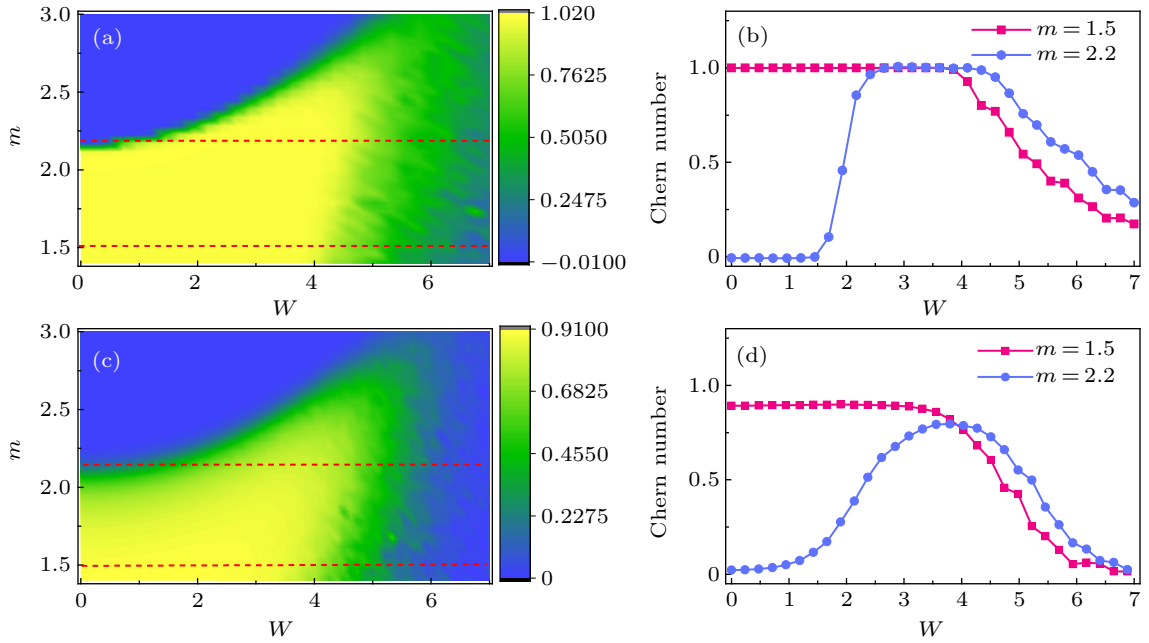


Fig. 4. (a), (c) The evolution of the Chern number with disorder strength W and m. (b), (d) denote the red dash line in (a), (c). (a), (b) is calculated by H_{eff} under the condition of periodic boundary. (c), (d) is calculated by H under the condition of open boundary. Parameters are set as $N = 30$ and $\gamma = 0.4$. The other parameters are the same as those in Fig. 2.

5. Disorder induced phase transition in cylindrical samples

In this section, we investigate the disorder-induced phase transition in cylindrical samples to further illustrate that NGM is also applicable to other non-Hermitian Hamiltonians. Following the study,[36] we use another Hamiltonian

$$H_{\text{C}} = (k_x + \mathrm{i}\gamma)\,\sigma_x + (k_y + \mathrm{i}\gamma)\,\sigma_y + [m - \cos(k_x + \mathrm{i}\gamma) - \cos(k_y + \mathrm{i}\gamma)]\,\sigma_z. \quad (7)$$

Since the open boundary condition only holds in one direction, one can take the replacement $k_y \to \tilde{k}_y - \mathrm{i}\gamma$, and the effective Hamiltonian can be expressed as[36]

$$H_{\mathrm{Ceff}} = (k_x + \mathrm{i}\gamma)\sigma_x + \tilde{k}_y\sigma_y + [m - \cos(k_x + \mathrm{i}\gamma) - \cos(\tilde{k}_y))]\sigma_z. \quad (8)$$

The phase boundary is predicated in the previous study[36]

$$m = 1 + \mathrm{e}^{\pm\gamma}. \quad (9)$$

First, the Chern number diagram evolving with m and γ is shown in Fig. 5(a), where the phase boundary obtained by numerical data follows the theoretical prediction $m = 1 + \mathrm{e}^{\pm\gamma}$ (marked by solid red lines). The two sides of the red line correspond to the topological state and trivial state, respectively, and the quantized characteristics of the Chern number are observed. The region separated by the two solid red lines in the figure corresponds to the gapless phase, which is also in consistent with our numerical results (i.e., in the region, the Chern number is neither quantized nor zero).

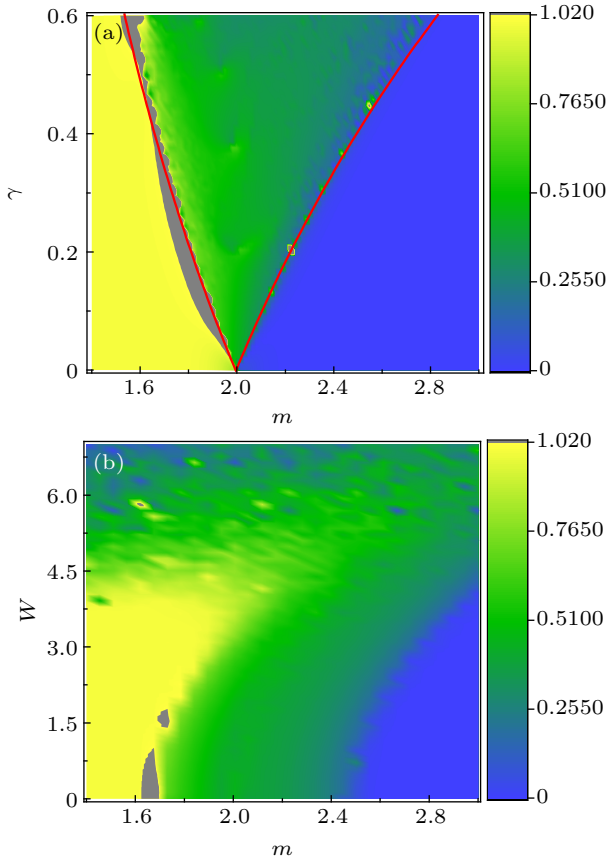


Fig. 5. (a) Chern number versus W and m of cylindrical samples, in which the red solid line is the phase boundary obtained by analytical results. (b) Chern number versus disorder strength W and m with $\gamma = 0.4$. The other parameters are the same as those in Fig. 2.

Then, we investigate the topological phase transition with the disorder. By setting $\gamma = 0.4$, the evolution of the Chern number is calculated. For a clean sample, the system has three different phases: when $m < 1 + \mathrm{e}^{-0.4}$, the system is topological nontrivial; when $m > 1 + \mathrm{e}^{0.4}$, the system is topological trivial; and when $1 + \mathrm{e}^{-0.4} < m < 1 + \mathrm{e}^{0.4}$, the system is gapless. With the increase of the disorder strength, the topological region with a quantized Chern number gradually extends to the gapless area. This specific Chern number evolution corresponds to a transition from the gapless phase to the topological Anderson insulator. Similarly, the gapless region gradually expands towards the normal insulator region with increasing disorder strength, which leads to the transition from the trivial phase to the gapless one. Besides, the area of the gapless phase is so vast that the topological nontrivial insulator state caused by disorder cannot extend to the insulator region. Thus, there exists no disorder-induced phase transition from a trivial state to a topological state in this case.

To better understand the influence of the non-Hermitian intensity on the topological phase transition, we set $W = 3$ and calculate the evolution of the Chern number by changing γ and m. The main results are shown in Fig. 6. Figure 6(a) is related to the cylindrical sample, where the solid red line is the phase boundary $(m = 1 + \mathrm{e}^{\pm\gamma})$ for the clean sample. The solid blue line separating the regions with a quantized and un-quantized Chern number in the figure is obtained by shifting the solid red line $m = 1 + \mathrm{e}^{-\gamma}$ about 0.2 along the m-axis. We have already known that the clean sample is in a gapless phase (the region between the solid red lines in Fig. 6(a)) when $1 + \mathrm{e}^{-\gamma} < m < 1 + \mathrm{e}^{\gamma}$. The left side of the solid red line is in a nontrivial topological phase, while the right side is in a trivial insulator phase. Hence, when $m > 1 + \mathrm{e}^{\gamma}$, the phase transition between the normal insulator and topological Anderson insulator corresponds to the region with a quantized Chern number. While the normal insulator phase to the gapless phase corresponds to the part with an un-quantized Chern number, and the remaining area corresponds to the normal insulator phase (blue zone) without a phase transition. Furthermore, only topological insulator exists under this disordered strength when $m < 1 + \mathrm{e}^{-\gamma}$. For $1 + \mathrm{e}^{-\gamma} < m < 1 + \mathrm{e}^{\gamma}$, the clean sample is in the gapless phase initially, but the Chern number becomes quantized by applying the disorder. The system undergoes a phase transition from the gapless phase to a topological insulator. Therefore, when the disorder strength changes from $W = 0$ to $W = 3$, the following phase transitions should happen: (1) the normal insulator phase to the gapless phase, (2) the normal insulator phase to the topological Anderson insulator phase, and (3) the gapless phase to the topological Anderson insulator phase. In contrast, for the case of the square sample (see Fig. 6(b)), only one kind of phase transition exists, which is from the normal insulator to the topological insulator. Furthermore, it seems that the non-Hermitian intensity, γ, has less influence on the topological Anderson transition for square samples. Oppositely, the phase transition

in cylindrical samples is sensitive to γ.

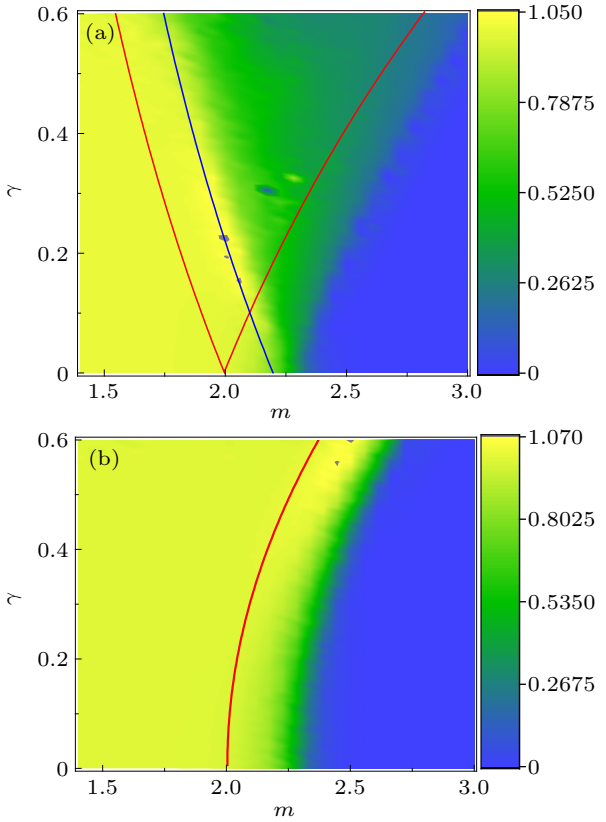


Fig. 6. Chern number versus γ and m with disorder strength $W = 3$. (a) is calculated by cylindrical samples. The solid red line is the phase boundary of the clean cylindrical sample, and the solid blue line roughly separates the regions with a quantized and un-quantized Chern number. (b) is calculated by the square sample, and the solid red line is the phase boundary of the clean sample. The other parameters are the same as those in Fig. 2.

6. Discussion and conclusion

A recent paper of Song *et al.*[67] also showed that the Chern number obtained in real space could be greater than one or less than zero, which is very similar to our results (see Fig. 3(a) in the grey area or Fig. 3(a) in the black area). For disordered Hermitian systems, the Chern number must be an integer. Thus, this strange Chern number evolution could be the feature of the non-Hermitian systems or just related to the inaccuracy of the numerical methods. In our viewpoint, we suspect the singular value of the Chern number is due to the fact that the equation $P_{\tilde{k}} = \sum_{n\in \mathrm{BZ}} b_n \mathrm{e}^{\mathrm{i}\tilde{k}n}$ could be inaccurate in non-Hermitian systems. Thus, it leads to the reduction of the accuracy of the Chern number. In order to make $P_{\tilde{k}} = \sum_{n\in \mathrm{BZ}} b_n \mathrm{e}^{\mathrm{i}\tilde{k}n}$ much reliable and the results more accurate, a large sample size is needed. In addition, the TAI phase in non-Hermitian systems is model-independent, and the existence of the TAI phase shows the interaction of disorder combined with non-Hermitian features. Similar results can also be obtained in other models after considering the self-energy induced by disorder. Furthermore, non-Hermitian samples may show different phase diagrams for different geometric structures. Therefore, the effect of disorder could be sensitive to the boundary conditions, which is unique for the non-Hermitian systems.

In summary, we investigate the applicability of NGM in the two-dimensional non-Hermitian system. By applying NGM, we study the disorder-induced phase transition in the two-dimensional non-Hermitian system, including both the situations of the square sample and the cylindrical sample. In the square sample, we find a disorder-induced direct phase transition from normal insulator to topological Anderson insulator. For the cylindrical sample, the system mainly has the following three phase transitions: (1) the normal insulator phase to the gapless phase, (2) the normal insulator phase to the topological Anderson insulator phase, and (3) the gapless phase to the topological Anderson insulator phase. We notice that a very recent paper proposed a method that can be used to investigate the topological index under the condition of open boundary[67] (a comparison of the methods in this paper and Ref. [67] is presented in appendix A). Besides, the topological Anderson transition in one-dimensional systems is also reported.[68]

Acknowledgement

We are grateful to Chui-Zhen Chen, Rui-Chun Xiao, Ye Xiong, and Yan-Zuo Kang for helpful discussion.

Appendix A

In this appendix, we will compare the similarities and differences between the NGM and the real-space Chern number method applied in Ref. [67]. In our previous paper,[55] a brief review of NGM has been given, and the Chern number in real space can be rewritten as[46,47,54,55,64,65]

$$C = -\frac{2\pi \mathrm{i}}{N^2} \sum_{n,\alpha} \langle n,\alpha | P\,[-\mathrm{i}\,[x_1, P], -\mathrm{i}\,[x_2, P]]\,|n,\alpha\rangle, \qquad \text{(A1)}$$

where P is the projection operator of the occupied states on the basis of real space and $|n,\alpha\rangle$ is the real space coordinates for orbit α. We notice that the real-space Chern number method applied in Ref. [67] is also based on NGM except that the summation of $|n,\alpha\rangle$ is not for all the sites. To deeply understand the differences, we plot the Chern number $C_n = \sum_\alpha -2\pi \mathrm{i} \langle n,\alpha | P[-\mathrm{i}\,[x_1,P], -\mathrm{i}\,[x_2,P]] | n,\alpha\rangle$ for each site $\sum_\alpha |n,\alpha\rangle$ in Fig. A1.

Figure A1(a) shows C_n for each site n with $\gamma = 0$ and $m = 1.5$. It is obvious that C_n is one under the periodic boundary ($\gamma = 0$) condition, and the average Chern number is one. While for the open boundary condition, the Chern number is smaller than one for some sites, and these sites are close to the sample's edge. The distribution of the Chern number for each site follows the same behavior (see Fig. A1(a)) when $\gamma = 0.4$. We also present a typical plot of C_n versus (N_x, N_y) under the

open boundary condition in Fig. A1(b), and it also manifests that C_n is smaller than one for sites near the edge. We believe the calculation of the Chern number in this paper and Ref. [67] could be the same until this step. Then, we considered all the sites in our calculation, and the average Chern number is smaller than one under the open boundary condition. While in Ref. [67], they only considered several sites that are far from the edge (as shown in Fig. A1(b) in the red dashed box), and the Chern number for these sites is still one. Therefore, the average Chern number is very close to the quantized one even under the open boundary conditions.

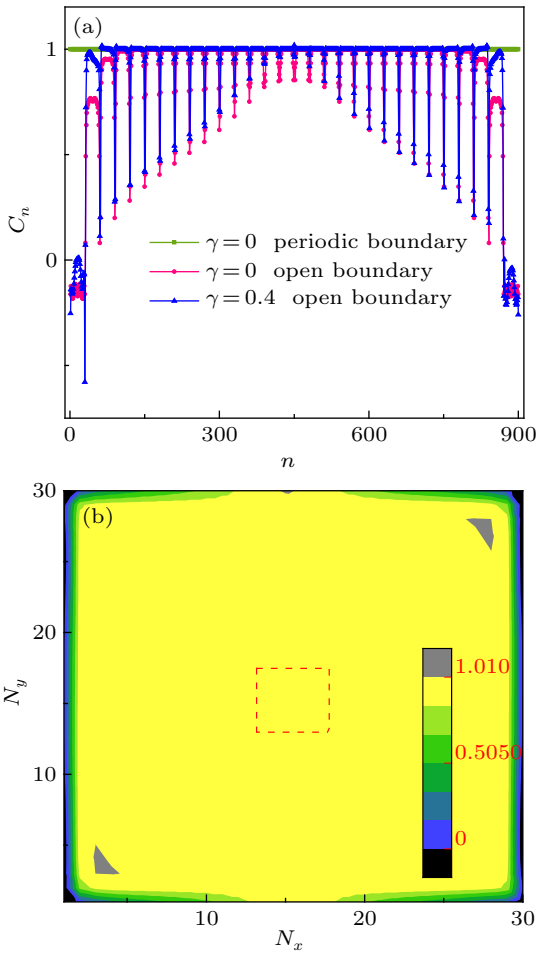


Fig. A1. Chern number $C_n=\sum_\alpha -2\pi \mathrm{i}\langle n,\alpha|P[-\mathrm{i}[x_1,P],-\mathrm{i}[x_2,P]]|n,\alpha\rangle$ for each site $\sum_\alpha|n,\alpha\rangle$ with $m=1.5$ and $N=30$. The Hamiltonian is shown in Eq. (1). (a) The plot of C_n versus n with $n=N_x+(N_y-1)N$. N_x and N_y are in the range $[1,N]$. (b) C_n versus (N_x,N_y) for the curve shown in (a) with $\gamma=0.4$ under the open boundary condition. The other parameters are the same as those in Fig. 2.

In summary, since the number of eigenstates is constant, the contribution of the bulk states decreases when edge states emerge. If one carefully select the bulk sites, the influences of the edge states can be eliminated, and the final Chern number will be much close to the quantized value.

References

[1] Kane C L and Mele E J 2005 *Phys. Rev. Lett.* **95** 226801
[2] Kane C L and Mele E J 2005 *Phys. Rev. Lett.* **95** 146802
[3] Hasan M Z, Kane C L and Colloquium 2010 *Rev. Mod. Phys.* **82** 3045
[4] Moore J E 2010 *Nature* **464** 194
[5] Qi X L and Zhang S C 2011 *Rev. Mod. Phys.* **83** 1057
[6] Bernevig B A, Hughes T L and Zhang S C 2006 *Science* **314** 1757
[7] König M, Wiedmann S, Brüne C, Roth A, Buhmann H, Molenkamp L W, Qi X L and Zhang S C 2007 *Science* **318** 766
[8] Yan B H and Felser C 2017 *Annu. Rev. Condens. Matter Phys.* **8** 337
[9] Liu Z K, Zhou B, Zhang Y, Wang Z J, Weng H M, Prabhakaran D, Mo S K, Shen Z X, Fang Z, Dai X, Hussain Z and Chen Y L 2014 *Science* **343** 864
[10] Alicea J 2012 *Rep. Prog. Phys.* **75** 076501
[11] Chang C Z, Zhang J, Feng X, Shen J, Zhang Z C, Guo M H, Li K, Ou Y B, Wei P, Wang L L, Ji Z Q, Feng Y, Ji S H, Chen X, Jia J F, Dai X, Fang Z, Zhang S C, He K, Wang Y Y, Lu L, Ma X C and Xue Q K 2013 *Science* **340** 167
[12] Schindler F, Cook A M, Vergniory M G, Wang Z, Parkin S S, Bernevig B and Neupert T 2018 *Sci. Adv.* **4** eaat0346
[13] Otrokov M M, Rusinov I P, Blanco-Rey M, Hoffmann M, Yu A, Eremeev S V, Ernst A, Echenique P M, Arnau A and Chulkov E V 2019 *Phys. Rev. Lett.* **122** 107202
[14] Altland A and Zirnbauer M R 1997 *Phys. Rev. B* **55** 1142
[15] Chiu C K, Teo J C Y, Schnyder A P and Ryu S 2016 *Rev. Mod. Phys.* **88** 035005
[16] Kitaev A 2009 *AIP Conf. Proc.* **1134** 22
[17] Fu L 2011 *Phys. Rev. Lett.* **106** 106802
[18] Hsieh T H, Lin H, Liu J W, Duan W H, Bansil A and Fu L 2012 *Nat. Commun.* **3** 982
[19] Dziawa P, Kowalski B J, Dybko K, Buczko R, Szczerbakow A, Szot M, Lusakowska E, Balasubramanian T, Wojek B M, Berntsen M H, Tjernberg O and Story T 2012 *Nat. Materials* **11** 1023
[20] Ando Y and Fu L 2015 *Annu. Rev. Condens. Matter Phys.* **6** 361
[21] Ma J Z, Yi C J, Lv B Q, Wang Z J, Nie S M, Wang L, Kong L Y, Huang Y B, Richard P, Zhang P, Yaji K, Kuroda K, Shin S, Weng H M, Bernevig B A, Shi Y G, Qian T and Ding H 2017 *Science Advances* **3** e1602415
[22] Wang Z, Alexandradinata A, Cava R J and Bernevig B A 2016 *Nature* **532** 189
[23] Po H C, Vishwanath A and Watanabe H 2017 *Nat. Commun.* **8** 50
[24] Bradlyn B, Elcoro L, Cano J, Vergniory M G, Wang Z J, Felser C, Aroyo M I and Bernevig B A 2017 *Nature* **547** 298
[25] Li Y H, Liu J, Song J T, Jiang H, Sun Q F and Xie X C 2018 *Sci. China-Phys: Mech. Astron.* **61** 97411
[26] Tang F, Po H C, Vishwanath A and Wan X G 2019 *Nature* **566** 486
[27] Zhang T, Jiang J, Song Z, Huang H, He Y Q, Fang Z, Weng H M and Fang C 2019 *Nature* **566** 475
[28] Vergniory M G, Elcoro L, Felser C, Regnault N, Bernevig B A and Wang Z J 2019 *Nature* **566** 480
[29] Moiseyev N 2011 *Non-Hermitian quantum mechanics* (London: Cambridge University Press) p. 211
[30] Graf G M and Porta M 2013 *Commun. Math. Phys.* **324** 851
[31] Shen H, Zhen B and Fu L 2018 *Phys. Rev. Lett.* **120** 146402
[32] Yin C H, Jiang H, Li L H, Lü R and Chen S 2018 *Phys. Rev. A* **97** 052115
[33] Xiong Y 2018 *J. Phys. Commun.* **2** 035043
[34] Kunst F K, Edvardsson E, Budich J C and Bergholtz E J 2018 *Phys. Rev. Lett.* **121** 026808
[35] Yao S and Wang Z 2018 *Phys. Rev. Lett.* **121** 086803
[36] Yao S, Song F and Wang Z 2018 *Phys. Rev. Lett.* **121** 136802
[37] Liu J S, Han Y Z and Liu C S 2020 *Chin. Phys. B* **29** 010302
[38] Zhao L Y, Li H W, Yin Z Q, Chen W, You J and Han Z F 2019 *Chin. Phys. B* **28** 100304
[39] Wang Y Y and Fang M F 2018 *Chin. Phys. B* **27** 114207
[40] Baradaran M and Panahi H 2017 *Chin. Phys. B* **26** 060301
[41] Song F, Yao S and Wang Z 2019 *Phys. Rev. Lett.* **123** 170401
[42] Zhang K, Yang Z and Fang C 2019 arXiv:1910.01131[hep-ph]
[43] Okuma N, Kawabata K, Shiozaki K and Sato M 2020 *Phys. Rev. Lett.* **124** 086801
[44] Fradkin E and Hirsch J E 1983 *Phys. Rev. B* **27** 1680
[45] Asbóth J K, Oroszlány L and Pályi A 2016 *The Su-Schrieffer-Heeger (SSH) Model*, in A Short Course on Topological Insulators: Band Structure and Edge States in One and Two Dimensions (Cham: Springer) pp. 1–22

[46] Mondragon-Shem I, Hughes T L, Song J T and Prodan E 2014 *Phys. Rev. Lett.* **113** 046802
[47] Song J T and Prodan E 2014 *Phys. Rev. B* **89** 224203
[48] Anderson P W 1958 *Phys. Rev.* **109** 1492
[49] Evers F and Mirlin A D 2008 *Rev. Mod. Phys.* **80** 1355
[50] Kramer B and MacKinnon A 1993 *Rep. Prog. Phys.* **56** 1469
[51] Lee P A and Ramakrishnan T V 1985 *Rev. Mod. Phy.* **57** 287
[52] Cha M C and Fertig H A 1995 *Phy. Rev. Lett.* **74** 4867
[53] Chen R, Xu D H and Zhou B 2017 *Phys. Rev. B* **96** 205304
[54] Zhang Z Q, Wu B L, Song J and Jiang H 2019 *Phys. Rev. B* **100** 184202
[55] Su Z X, Kang Y Z, Zhang B F, Zhang Z Q and Jiang H 2019 *Chin. Phys. B* **28** 117301
[56] Wu B L, Song J T, Zhou J J and Jiang H 2016 *Chin. Phys. B* **25** 117311
[57] Li J, Chu R L, Jain J K and Shen S Q 2009 *Phys. Rev. Lett.* **102** 136806
[58] Jiang H, Wang L, Sun Q F and Xie X C 2009 *Phys. Rev. B* **80** 165316
[59] Meier E J, An F A, Dauphin A, Maffei M, Massignan P 2018 *Science* **362** 929
[60] Stützer S, Plotnik Y, Lumer Y, Titum P, Lindner N H, Segev M, Rechtsman M C and Szameit A 2018 *Nature* **560** 461
[61] Gong Z P, Ashida Y T, Kawabata K, Takasan K, Higashikawa S and Ueda M 2018 *Phys. Rev. X* **8** 031079
[62] Alvarez V M M, Vargas J E B and Torres L E F F 2018 *Phys. Rev. B* **97** 121401
[63] Tzortzakakis A F, Makris K G and Economou E 2020 *Phys. Rev. B* **101** 014202
[64] Prodan E 2011 *Phys. A-Math. Theor.* **44** 113001
[65] Zhang Y F, Yang Y Y, Ju Y, Sheng L, Shen R, Sheng D N and Xing D Y 2013 *Chin. Phys. B* **22** 117312
[66] Kawabata K, Shiozaki K, Ueda M and Sato M 2019 *Phys. Rev. X* **9** 041015
[67] Song F, Yao S and Wang Z 2019 *Phys. Rev. Lett.* **123** 246801
[68] Zhang D W, Tang L Z, Lang L J, Yan H and Zhu S L 2019 arXiv:1908.01172[hep-ph]